Characterization and Reactivity of Copper Oxide Catalysts Supported on TiO_2-ZrO_2

Komandur V. R. Chary,* Guggilla Vidya Sagar, Dhachapally Naresh, Kottapalli Kalyana Seela, and Bojja Sridhar

Catalysis Division, Indian Institute of Chemical Technology, Hyderabad 500 007, India

Received: January 3, 2005; In Final Form: March 7, 2005

A series of copper catalysts supported on TiO_2-ZrO_2 with copper loading varying from 1.0 to 21.6 wt % were prepared by a wet impregnation method. The catalysts were characterized by X-ray diffraction (XRD), X-ray photoelectron spectroscopy (XPS), UV−vis diffuse reflectance spectroscopy, electron spin resonance (ESR), temperature programmed reduction (TPR), and Brunauer−Emmett−Teller specific surface area measurements. Copper dispersion and metal area were determined by N_2O decomposition by the passivation method. XRD results suggest that the copper oxide is present in a highly dispersed amorphous state at copper loadings <16.8 wt % in the sample and as a crystalline CuO phase at higher Cu loadings. Copper dispersion increases with Cu loading up to 5.1 wt % and levels off at higher loadings. The XPS peak intensity ratios of Cu $2p_{3/2}$/Ti $2p_{3/2}$ and Cu $2p_{3/2}$/Zr $3d_{5/2}$ were compared with the copper dispersion calculated from N_2O decomposition. ESR results suggest the presence of two types of copper species on the TiO_2-ZrO_2 support. TPR profiles reveal the presence of highly dispersed copper oxide at lower temperatures and bulk CuO at higher temperatures. The catalytic properties were evaluated for the vapor-phase dehydrogenation of cyclohexanol to cyclohexanone and related to the dispersion of Cu on TiO_2-ZrO_2.

1. Introduction

Supported copper catalysts catalyze many industrially important reactions. Copper catalysts are widely employed commercially for the dehydrogenation of higher alcohols to aldehydes and ketones, cyclohexanol to cyclohexanone,[1−3] the synthesis of methanol,[4] the direct decomposition of N_2O to N_2,[5−7] the selective catalytic reduction of nitrogen oxides by hydrocarbons in an oxygen-rich atmosphere,[8,9] CO oxidation,[10] the hydrogenolysis of esters,[11] and also for the conversion of CO_2 to CO by catalytic hydrogenation.[12] In addition, they can also be used in hydrogen fuel cells to generate energy for vehicles.[13−15] The catalytic properties of the active copper phase can be greatly influenced by the nature of the supported oxide and the dispersion of the active component.[16] However, the nature of the active species of these catalysts is still the subject of extensive investigation by many researchers.

The catalytic dehydrogenation of alcohol on metallic copper catalysts has been studied for decades due to its practical importance in the chemical industry. The dehydrogenation of cyclohexanol to cyclohexanone is an industrially important reaction in the manufacture of Nylon 6,6.[17,18] This is so because the two major raw materials for the production of polyamide fiber are caprolactam and adipic acid, both of which can be obtained from cyclohexanone, which is conventionally produced via the direct dehydrogenation of cyclohexanol over ZnO- or Cu-based catalysts.[18−20] Copper-based catalysts have been used extensively in the dehydrogenation reaction.[21,22] Since direct dehydrogenation is an endothermic reaction and is limited by the equilibrium thermodynamic limitation, high reaction temperatures are required, and typical conversions are found to be low.[18] These conditions can also lead to catalyst sintering and deactivation.[17,18,22−23] For these reasons, there has been a great deal of interest in developing oxidative dehydrogenation reactions.[24−26] Cyclohexene is usually the main side product of the dehydrogenation reaction of cyclohexanol, and the selectivity of this reaction is known to be related to the catalyst acid functionality. Indeed, the selectivity to cyclohexanone increases by decreasing the acidity of the catalyst.[17,18,21,22]

Attempts to develop highly active and thermostable dehydrogenation catalysts have been carried out recently.[21−23] In many instances, the active CuO is supported on oxides such as Al_2O_3, SiO_2, ZrO_2, and TiO_2 in combination with Zn or other transition metals such as Ru and Fe. The disadvantages of these supports are their low surface areas, high surface acidities, low activities, and phase transitions at higher temperatures, which make them unsuitable for industrial applications. The use of mixed oxide support or stabilization of these supports can overcome these problems. In the recent past, the mixed oxide supports have been synthesized by coprecipitation, and sol−gel methods have been the subject of a number of investigations. The catalytic activities of TiO_2-based catalysts for various kinds of reactions have been described in a review by Matsuda and Kato.[27] The correlation between catalytic activity and acidic and basic properties of TiO_2,[28] ZrO_2,[29] and TiO_2-ZrO_2[29−32] have been investigated extensively. The TiO_2-ZrO_2 mixed oxide seems to be an interesting support material for vanadia and is employed in the cyclohexene oxide isomerization to allyl alcohols,[32] the dehydrogenation of ethyl benzene to styrene,[33,34] or the dehydrocyclization of C_6-C_8 *n*-paraffins to aromatics.[35] They have also been tested as a support for platinum in the reforming of *n*-hexane and nitric oxide reduction with methane.[36,37] Hence, the characterization of TiO_2-ZrO_2-supported catalysts is very important to discuss for the catalytic activity and for the prediction of the catalyst performance (activity and selectivity) in various reactions.

In the present investigation, we report the effect of copper loading in CuO/TiO_2-ZrO_2 catalysts by X-ray diffraction

* Author to whom correspondence should be addressed. Phone: +91-40-27193162. Fax: +91-40-27160921. E-mail: kvrchary@iict.res.in.

10.1021/jp0500135 CCC: $30.25
Published on Web 04/14/2005

(XRD), UV−vis diffuse reflectance spectroscopy (UV-DRS), electron spin resonance (ESR), X-ray photoelectron spectroscopy (XPS), temperature programmed reduction (TPR), Cu dispersion, and determination of the metal area by N_2O decomposition. We also report the activity and selectivity of the catalysts in the dehydrogenation of cyclohexanol to cyclohexanone in comparison with the dispersion of Cu.

2. Experimental Section

The TiO_2-ZrO_2 mixed oxide (1:1 wt %) support was prepared by the coprecipitation method. The requisite quantities of titanium isopropoxide in 2-propanol, zirconium(IV) propoxide in propanol, and NH_3 (40% aqueous solution) were continuously stirred for 6 h at 343 K. The precipitation was completed after 4−5 h of stirring at which the pH of the solution was 9. The precipitate thus obtained was then filtered, washed several times with deionized water until it was free from the base, dried overnight at 393 K, and finally calcined at 773 K for 6 h.

A series of copper catalysts with Cu loadings varying from 1 to 21.6 wt % were prepared by wet impregnation of $Cu(NO_3)_2 \cdot 3H_2O$ (Fluka) on the support TiO_2-ZrO_2 (Brunauer−Emmett−Teller (BET) specific surface area 170 m^2/g). The samples were dried at 383 K for 16 h and subsequently calcined at 773 K for 5 h in air.

The copper content was determined by atomic absorption spectroscopy, using a Perkin-Elmer Analyst 300 double-beam spectrometer. The powders were first dissolved in acidic solution (40% HF) and diluted to concentrations within the detection range of the instrument.

X-ray powder diffraction patterns were obtained with a Siemens D5000 diffractometer, using Cu Kα radiation (1.5406 Å) at 40 kV and 30 mA and a secondary graphite monochromator. The measurements were recorded in steps of 0.045° with a count time of 0.5 s in the 2θ range of 2−65°. Identification of the phase was made with the help of the Joint Committee on Powder Diffraction Standards (JCPDS) files.

The specific surface area of the catalyst samples were estimated using the N_2 adsorption isotherm at 77 K by the single-point BET method using a Micromeritics Pluse Chemisorb 2700 instrument. Before measurements, the samples were oven-dried at 393 K for 12 h and flushed in situ with He gas for 2 h.

UV−vis spectra were recorded in air at room temperature using a GBC UV−vis Cintra 10e spectrometer with a diffuse reflectance accessory, in the 200−800 nm wavelength range. The TiO_2-ZrO_2 support was used as a reference. The Kubelka−Munk function $F(R)$ was plotted against the wavelength (in nm).

ESR spectra of the precalcined samples were recorded on a Bruker EMX-X band spectrometer at the X-band frequency 9.7667 GHz at 293 K. The spectra were calibrated with an ER 035M NMR Gauss meter.

XPS was used to study the chemical composition and oxidation state of the catalyst surfaces. The XPS spectra of the catalysts were measured on a XPS spectrometer (Kratos-Axis 165) with Mg Kα radiation ($h\nu = 1253.6$ eV) at 75 W. The Cu 2p, Ti 2p, and Zr 3d core-level spectra were recorded, and the corresponding binding energies were referenced to the C 1s line at 284.6 eV (accuracy within ±0.2 eV). The background pressure during the data acquisition was kept below 10^{-10} bar.

TPR studies were carried out on an Auto Chem 2910 (Micromeritics) instrument to study the copper dispersion and reducibility. In a typical experiment, 300 mg of oven-dried sample (dried at 373 K for 15 h) was taken in a U-shaped quartz sample tube. The catalyst was mounted on a quartz wool plug. Prior to TPR studies, helium gas was passed with a flow rate of 50 mL/min at 393 K for 2 h to pretreat the catalyst sample. After pretreatment, the sample was cooled to ambient temperature, and TPR analysis was carried out in a flow of 10% H_2-Ar (50 mL/min) from ambient temperature to 623 K at a heating rate of 10 K/min. H_2 consumption and T_{max} positions were calculated using the GRAMS/32 software.

Copper surface area, percentage dispersion, and Cu crystallite size were calculated by N_2O decomposition conducted on an Auto Chem 2910 (Micromeritics). This method was based on the decomposition of N_2O over a metallic surface, which releases N_2.[38] The catalysts were pretreated in a helium flow (50 mL/min) and heated at 393 K for 30 min. The catalysts were reduced with a flow mixture of 10% H_2-Ar, raising the temperature at a heating rate of 10 K/min up to 623 K. In sequence, oxidation with N_2O was performed at 333 K for 45 min flowing N_2O (50 mL/min). Reduction of the surface oxide sublayer was performed similarly as in TPR, raising the temperature up to 623 K.

Temperature programmed desorption (TPD) experiments were also conducted on an Auto Chem 2910 instrument. In a typical experiment for TPD studies, the sample was pretreated by passage of high-purity (99.995%) helium (50 mL/min) at 473 K for 1 h. After pretreatment, the sample was saturated with high-purity anhydrous ammonia (75 mL/min) with a mixture of 10% NH_3-He at 353 K for 1 h and subsequently flushed with He flow (50 mL/min) at 378 K for 2 h to remove physisorbed ammonia. TPD analysis was carried out from ambient temperature to 1023 K at a heating rate of 10 K/min. The amount of NH_3 desorbed was calculated using the GRAMS/32 software.

A down-flow fixed-bed reactor operating at atmospheric pressure and made of Pyrex glass was used to test the catalysts during the dehydrogenation of cyclohexanol to cyclohexanone. Approximately 500 mg of the catalyst diluted with an equal amount of quartz grains was charged into the reactor and was supported on a glass wool bed. Prior to the introduction of the reactant cyclohexanol with a syringe pump, the catalyst was reduced at 523 K for 3 h, in purified hydrogen flow. After the prereduction, the reactor was fed with cyclohexanol at 523 K in N_2 (flow rate 50 mL/min), which is used as the carrier gas. The liquid products, mainly cyclohexanone and cyclohexene, were analyzed by a Hewlett-Packard 6890 gas chromatograph equipped with a flame ionization detector using a HP-5 capillary column. The products were also identified using a HP 5973 quadruple GC-MSD system using a HP-1MS capillary column.

3. Results and Discussion

The X- ray diffraction patterns of CuO catalysts supported on TiO_2-ZrO_2 calcined at 773 K are shown in Figure 1. In all of the samples, no diffraction lines due to ZrO_2 or TiO_2 were observed in the XRD pattern of the CuO/TiO_2-ZrO_2 (1:1) catalysts, which confirms that the TiO_2-ZrO_2 phase is an amorphous or poorly crystalline material. The XRD patterns suggest that there are no detectable diffraction peaks representing crystalline CuO in the sample with Cu loading less than 16.8 wt %, which clearly indicates that a copper oxide species is present in a highly dispersed amorphous state. However, it cannot be ruled out that the CuO crystallites might be present as small crystallites of <4 nm in diameter, which are undetectable by XRD. At higher Cu loadings (from 16.8 wt % of Cu), XRD reflections due to crystalline CuO are noticed at $2\theta = 35.5°$ ($d = 2.52$ Å) and 38.7° ($d = 2.38$ Å), and the intensities of these reflections are found to increase with the increase of Cu loading. The XRD patterns also indicate that no characteristic

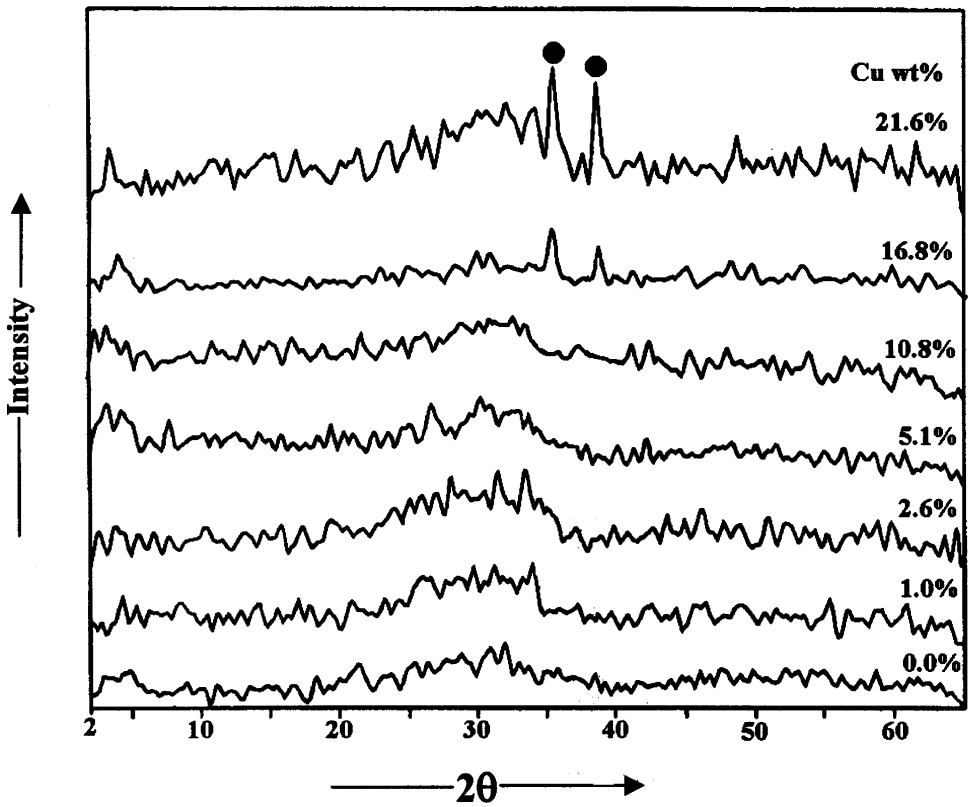

Figure 1. X-ray diffractograms of various CuO/TiO_2-ZrO_2 catalysts (● due to CuO).

peaks were found due to the formation of a mixed oxide phase between CuO and the TiO_2-ZrO_2 support.

The BET surface areas of various catalysts are reported in Table 3. The specific surface area of the pure TiO_2-ZrO_2 support was found to be 170 m^2/g. The decrease in the BET surface area of the Cu/TiO_2-ZrO_2-supported catalysts with the increase in copper loading is presumably as a result of the plugging of the pores by crystallites of CuO as shown by the results of X-ray diffraction.

The UV−vis spectra of CuO/TiO_2-ZrO_2 calcined samples are shown in Figure 2. No other peaks were observed except around 300 nm in the DR spectra of the TiO_2-ZrO_2 support without copper. The DR spectrum of the CuO/TiO_2-ZrO_2 catalysts show strong absorption bands at 210−270 and 357 nm and a large absorption band at 600−800 nm. The charge-transfer (CT) bands give us an idea of the environment in the neighborhood of Cu^{2+} ions. According to the literature,[18,39,40] the band at 210−270 nm indicates the $O^{2-} \rightarrow Cu^{2+}$ ligand-to-metal charge-transfer (LMCT) transition, where the Cu ions occupy isolated sites over the support. The absence of the 210−270 nm band in the DR spectrum for 1 wt % Cu catalyst is probably due to it being below the detection limit. The band at 357 nm indicates the formation of $(Cu-O-Cu)^{2+}$ clusters in a highly dispersed state, which is not detectable by XRD. The large absorption band at 600−800 nm is assigned to $^2E_g \rightarrow {}^2T_{2g}$ transitions of Cu^{2+} situated in the distorted octahedral symmetry. Although the DR spectra in the present study have been recorded in air atmosphere, the formation of such Cu^+ species in these samples cannot be discarded. According to an earlier report,[39] strong absorption bands at 210−350 and 400−500 nm and weak absorption band at 600−900 nm characterized impregnated copper−alumina samples. Mendes et al.[41] have observed that the broad band between 600 and 900 nm and the band at 350 nm indicate the formation of copper clusters different from bulk CuO. The intensities of the broad absorption band between 600 and 800 nm, which increases with Cu loading, and the strong absorption band between 210 and

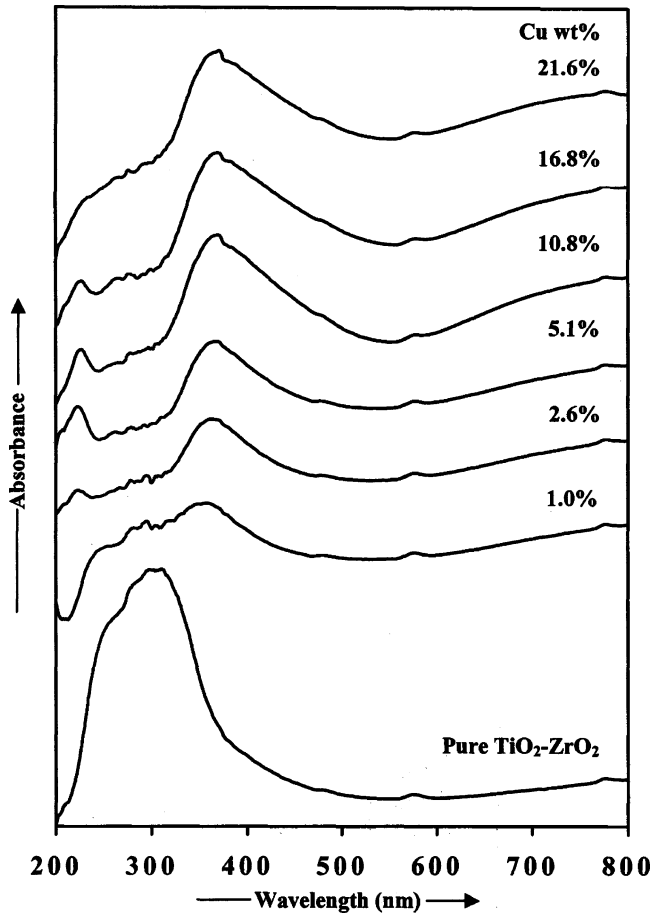

Figure 2. UV−vis diffuse reflectance spectra of various CuO/TiO_2-ZrO_2 catalysts.

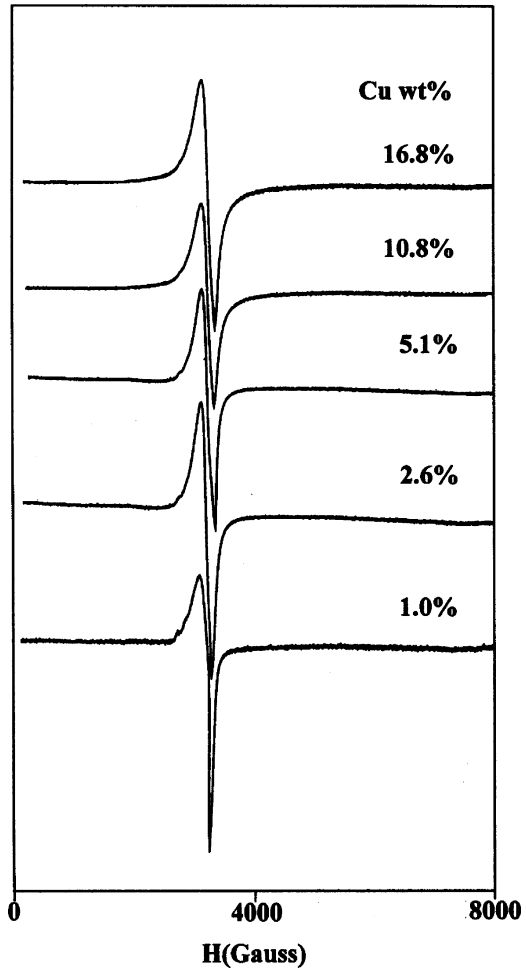

Figure 3. Electron spin resonance spectra of various calcined CuO/TiO_2-ZrO_2 catalysts.

TABLE 1: ESR Parameters of the CuO/TiO_2-ZrO_2 Catalysts

sample no.	Cu wt %	$g^{\|}$	$A^{\|}$	$g^{\perp}$	$A^{\perp}$
1	1.0	2.42	100	2.06	146
2	2.6	2.37	110	2.07	136
3	5.1	2.10	108	2.06	133
4	10.8	2.38	112	2.06	150
5	16.8	2.31	114	2.06	153

270, which decreases with Cu loading, clearly suggest the increase of crystalline and bulk CuO. This is also in good agreement with the previous observation that the intensities of the XRD peaks increased with the increase of Cu loading.

The d−d transition of the Cu^{II} ion in the presence of the ligand (or crystal) field generated by ligand or oxygen ions has been reported to appear in the visible or near-infrared range.[42] For an octahedral environment, transitions appear from 600 to 800 nm, depending on the ligand field strength. For tetrahedral symmetry, transitions are located in the spectral range between 100 and 1600 nm.[43] Iwamoto and his group[44] have reported that the peaks at 320 and 440 nm in the DR spectra of Cu-ZSM-5 zeolites were identified as $Cu^{II}-O^-$ and $(Cu-O-Cu)^{2+}$, respectively.

ESR is an important technique to investigate the Cu^{2+} species in the catalysts. The room-temperature ESR spectra of calcined samples are shown in Figure 3. In all samples, the spectra showed the presence of two kinds of ESR signals. The first one is an axial signal with a resolved hyperfine structure visible in the parallel component and typical of Cu^{2+}-containing systems. The

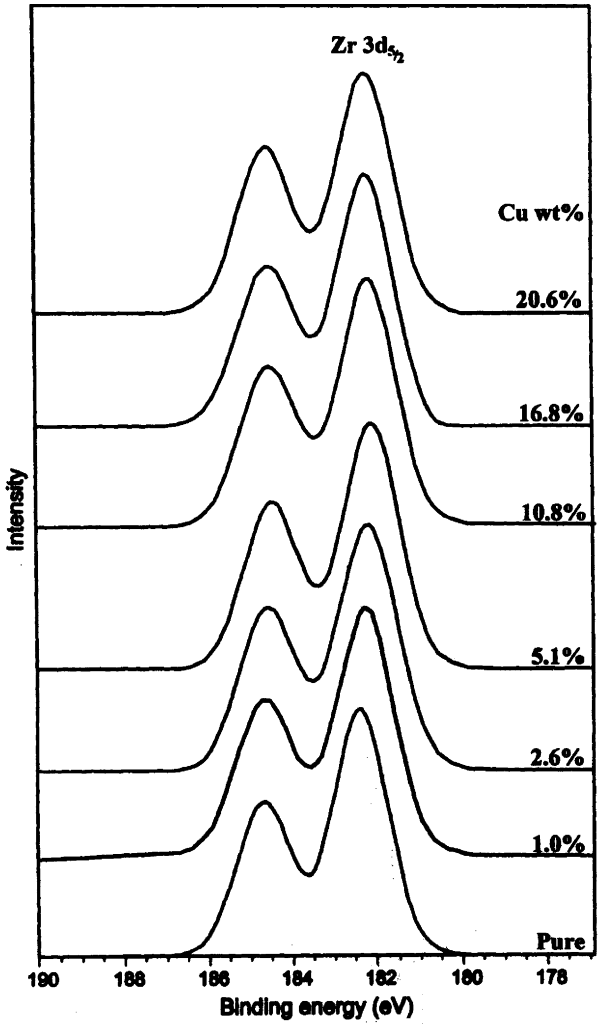

Figure 4. Zr 3d XPS spectra of the TiO_2-ZrO_2 support and various CuO/TiO_2-ZrO_2 catalysts.

ESR peaks of Cu^{2+} ($m_I = -1/2, -3/2$) in the low magnetic field are due to the parallel components. The second signal is broad, unstructured, and slightly axial. The spectra actually observed are partially resolved in the parallel component only. The resolution decreases with increasing copper content. The spin Hamiltonian parameters for both the signals were evaluated and are given in Table 1. The first signal can be attributed to isolated or nearly isolated copper ions in axial symmetry, probably an axially distorted octahedral environment, and its parameters are close to those previously reported for copper−alumina,[45,46] copper−zirconia,[47] copper−ceria−zirconia,[48] and copper−niobia[49] systems. The second signal showing an unresolved hyperfine splitting could be attributed to the Cu^{2+} species interacting with each other and generally are referred to as clustered Cu^{2+} ions. The results of Table 1 reveal that there are two types of Cu^{2+} ions, which are chemically inequivalent. The anisotropic signal intensity decreased with an increase in Cu content. This may be due to the formation of aggregates by spin-pairing that occurs when the distance between the ions is too close, resulting in dipolar broadening, which can be shown by UV-DRS and also by XRD. The Cu^{2+} hyperfine splitting observed in the catalyst (1 wt % Cu) reveals the isolated nature of the copper ions.

The catalyst surface composition was investigated by XPS. Figures 4, 5, and 6 show Zr 3d, Ti 2p, and Cu 2p XPS of various CuO/TiO_2-ZrO_2 calcined catalysts. The Zr $3d_{5/2}$ and Zr $3d_{3/2}$

TABLE 2: Binding Energies (eV), fwhm, XPS Atomic Ratios of Zr $3d_{5/2}$, Ti $2p_{3/2}$, and Cu $2p_{3/2}$ for CuO/TiO_2-ZrO_2 Catalysts

Cu wt % on TiO_2-ZrO_2	position and fwhm of Zr $3d_{5/2}$	position and fwhm of Ti $2p_{3/2}$	position and fwhm of Cu $2p_{3/2}$	XPS intensity Cu 2p/Zr 3d	XPS intensity Cu 2p/Ti 2p
0.0	182.3(1.5)[a]	458.6(1.6)[a]			
1.0	182.3(1.5)	458.6(1.7)	932.2(3.4)[a]	0.20	0.20
2.6	182.2(1.6)	458.6(1.6)	932.9(3.4)	0.22	0.21
5.1	182.2(1.5)	458.5(1.6)	933.5(3.1)	0.25	0.23
10.8	182.2(1.5)	458.5(1.7)	933.2(2.9)	0.43	0.45
16.8	182.2(1.5)	458.6(1.6)	934.2(3.1)	0.61	0.52
21.6	182.2(1.5)	458.5(1.6)	934.2(3.7)	0.62	0.51

[a] The numbers in parentheses are fwhm values.

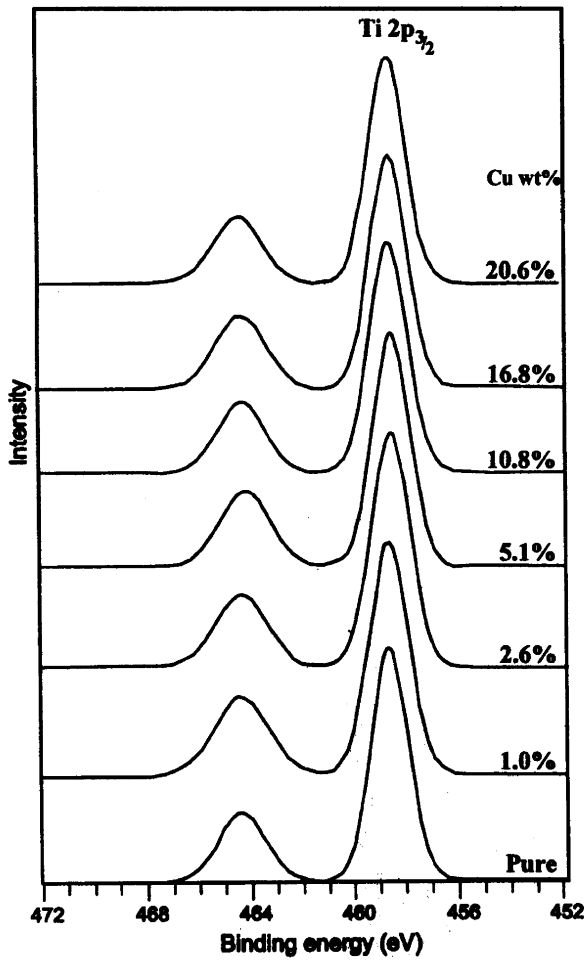

Figure 5. Ti 2p XPS spectra of the TiO_2-ZrO_2 support and various CuO/TiO_2-ZrO_2 catalysts.

binding energy values are in the range of 182.2 and 185.0 eV, respectively. The binding energies of Zr $3d_{5/2}$ and its full width at half-maximum (fwhm) values are reported in Table 2. The constant fwhm values are around 1.5, implying that only one type of doublet is present. This provides evidence for the presence of a single type of zirconium oxide with an oxidation state of 4+. The intensities of the Zr 3d core-level spectra do not change much with the increase in copper loading. Figure 5 shows the binding energies of Ti 2p in the range of 458.6 eV for Ti $2p_{3/2}$, which is in agreement with the values reported in the literature.[50] The binding energy values of Zr 3d and Ti 2p do not change much with varying copper loadings, indicating the integrity of the support structure, which was not modified by copper impregnation. The binding energies of Ti $2p_{3/2}$ and its fwhm values are reported in Table 2. The constant binding energies of Ti $2p_{3/2}$ and its fwhm values indicate the presence of one type of titanium oxide with an oxidation state of 4+.

Figure 6 shows Cu 2p XPS of various CuO/TiO_2-ZrO_2 catalysts. The binding energy of the Cu $2p_{3/2}$ peak at 934.2 eV together with the peak half-width of 3.8 eV and the characteristic shakeup feature at a binding energy of 944 eV are indicative of Cu^{2+} species,[51] while lower binding energy (932.2−933.1 eV) and the absence of shakeup peaks is characteristic of Cu^{1+}.[52] The binding energy and fwhm values of Cu $2p_{3/2}$ peaks are listed in Table 2 for different copper loadings. Our results indicate that the copper species is present as Cu^{2+} in all of the catalysts as indicated by the shakeup peaks in Figure 6. The absence of shakeup peaks in the XPS spectra at low Cu loadings (1.0 and 2.6 wt % of Cu) might be due to the presence of CuO in a highly dispersed amorphous state. However, the measured binding energy is slightly higher than that for Cu_2O. It is known that nanosized particles have properties different from the bulk oxides, and this mixed oxidation state could be the result of the defective structure of the small clusters. The constant fwhm values are around 3.6, implying that only one type of triplet is present. This provides evidence for the presence of a single type of copper oxide with an oxidation state of 2+. The intensity of the Cu 2p core-level spectra increases with the increasing Cu loading and levels off at higher loadings. This is in good agreement with the previous observation that the intensities of the XRD peaks increased with the increasing Cu loading.

The XPS intensity ratios of Cu 2p/Ti 2p and Cu 2p/Zr 3d for various CuO/TiO_2-ZrO_2 catalysts are shown in Table 2. The XPS intensity ratios of Cu 2p/Ti 2p and Cu 2p/Zr 3d increase with the increasing copper loading with maxima at 10.8 wt % and did not change appreciably with further increases in the Cu loading. This could be due to the formation of large CuO crystallites. Detection of bulk CuO in the samples with 16.8 wt % and greater copper loadings was confirmed by the XRD patterns of these catalysts. The activities of the catalysts in the dehydrogenation of cyclohexanol to cyclohexanone were also found to increase up to 10.8 wt % loading and leveled off at higher loadings. Thus, a low dispersion of copper oxide is noticed at higher loadings by the N_2O decomposition method described later in this section. Thus, the present XPS results are in good agreement with the dispersion of copper determined by the N_2O decomposition method.

The reducibility of copper species in the CuO/TiO_2-ZrO_2 catalysts was investigated by TPR experiments, and the profiles are shown in Figure 7. In all the samples, reduction profiles changed as the copper loadings increased. In the CuO/TiO_2-ZrO_2 catalysts, two different Cu species were observed. Yan et al.[53] reported similar observations in their study of the deactivation of Cu-ZSM-5 zeolite catalysts for the selective catalytic reduction of NO and also compared the reduction of copper on various supports. It was reported that the surface copper oxide species on the support is more easily reduced than the bulk CuO.[54−57] The T_{max} position of the first peak shifts to low-temperature region with increasing Cu loading. In the sample containing 1 wt % of Cu, the Cu is

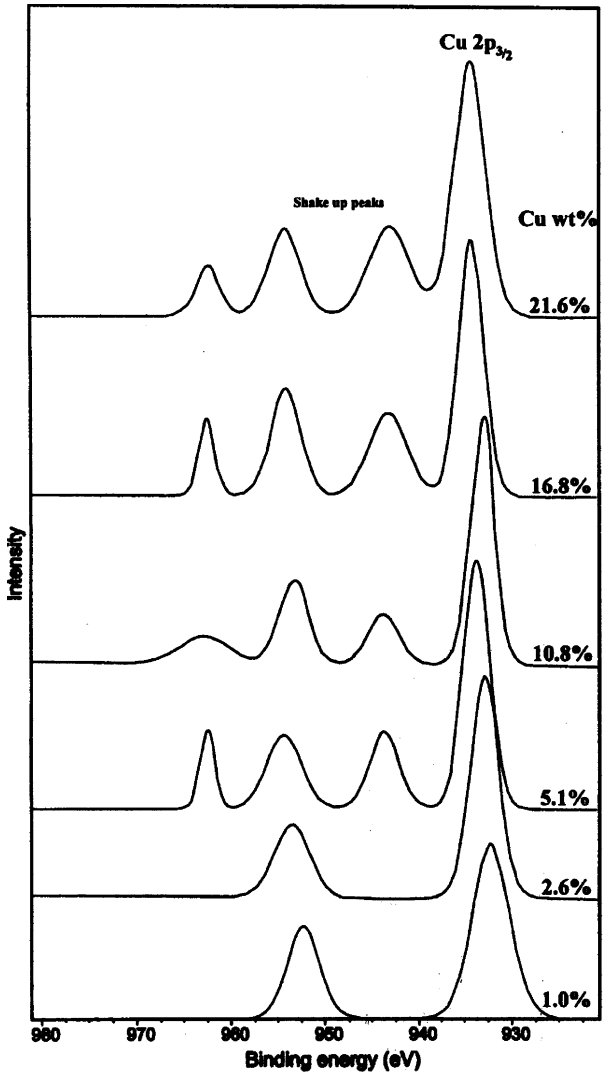

Figure 6. Cu 2p XPS spectra of various CuO/TiO_2-ZrO_2 catalysts.

present as highly dispersed clusters or as isolated Cu ions that strongly interact with the support, and reduction requires higher temperature of 564 K. It is also possible that reduction at low Cu contents requires diffusion of H_2 into the lattice or diffusion of lattice oxygen to the surface. When the copper loading is above 2.6 wt %, the first peak splits into two peaks. The first peak intensity increases with increasing copper loading up to 10.8 wt %; it seems to have a saturation phenomenon occurring at 10.8% Cu for the first peak. When the copper loading is higher than 10.8 wt %, the second peak was observed and obviously increases with increasing copper loadings. For the 16.8 wt % Cu/TiO_2-ZrO_2 catalyst, the TPR peaks in low-temperature region are attributed to the highly dispersed surface CuO species, and the TPR peak observed in the high-temperature region is attributed to the bulk CuO. The reduction peak is shifted toward high temperatures, and peaks become relatively broad with increasing Cu content. The broadening of the peak and the shifting of the T_{max} toward high temperatures may be due to the increasing crystallinity of CuO with the increase in Cu loading as shown from XRD results. The hydrogen consumption values and T_{max} during the TPR are given Table 3. It is observed that the H_2 consumption of the first peak is found to be highest for 10.8 wt % of Cu among all the samples. This clearly shows that the dispersion is high for 10.8 wt % and decreases with further copper loading.

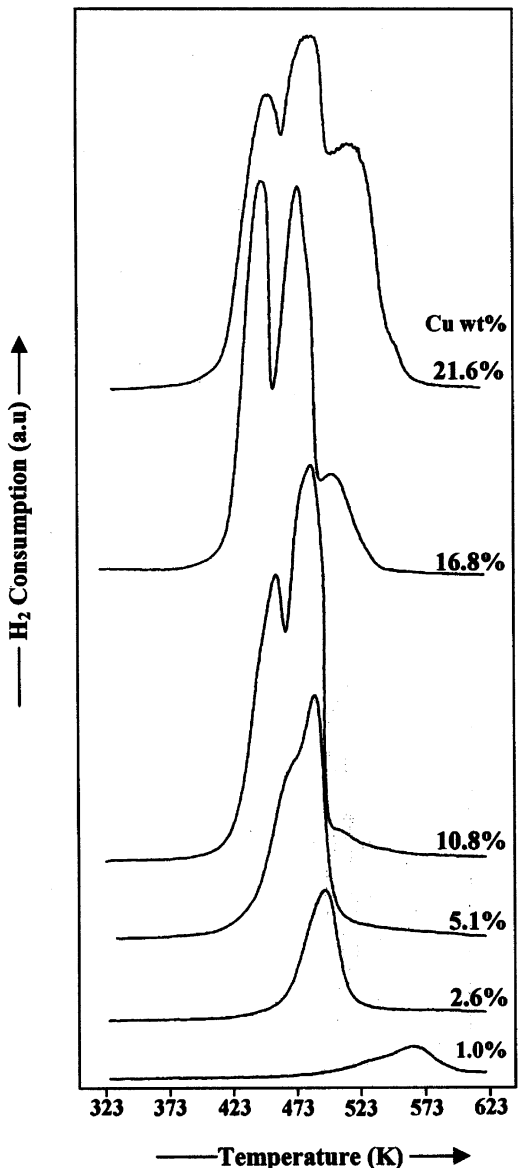

Figure 7. Temperature programmed reduction profiles of various CuO/TiO_2-ZrO_2 catalysts.

The dispersion and crystallite size[58,59] (assuming a spherical shape of the copper metal particles) values given in Table 4 are calculated from N_2O decomposition data using the following equations

$$N_2O_{(gas)} + 2Cu_{(s)} \rightarrow Cu_{(s)}-O-Cu_{(s)} + N_{2(gas)} \qquad (1)$$

$$\text{crystallite size (nm)} = 6000/(\text{Cu metal area per gram Cu} \times \text{Cu density}) \qquad (2)$$

where Cu density = 8.92 g/cm^3.

The copper metal areas were determined using the equation $S_H = n_m^s X_m n_s^{-1}$, where S_H is the total metallic surface area, n_m^s is the total number of nitrous oxide molecules decomposed, X_m is chemisorption stoichiometry at monolayer coverage, and n_s^{-1} is the number of copper metal atoms per unit area of surface (1.47×10^{19} m^{-2}). The Cu percentage dispersion, Cu metal area (m^2/g Cu), and crystallize size (nm) are given in Table 4. It was observed that the dispersion and metal areas increase and crystalline size decreases up to 5.1 wt % of Cu on TiO_2-ZrO_2. This might be due to the maximum number of dispersed copper sites that are available on the catalyst surface. However, beyond this loading, the CuO crystallites are formed, the

TABLE 3: BET Surface Area and Temperature Programmed Reduction Results of Various CuO/TiO_2-ZrO_2 Catalysts

sample no.	Cu wt %	BET surface area (m^2/g)	T_{max}^1 (K)	H_2 consumption[1] (μmol/g)	T_{max}^2 (K)	H_2 consumption[2] (μmol/g)	T_{max}^3 (K)	H_2 consumption[3] (μmol/g)
1	0.0	170						
2	1.0	147	564	124				
3	2.6	140	495	341				
4	5.1	136	477	368	485	375		
5	10.8	128	454	592	481	998		
6	16.8	119	436	886	465	1287	497	361
7	21.6	81	439	729	486	1352	512	1243

TABLE 4: Dispersion, Copper Metal Area, Average Particle Size, and Activity Results for CuO/TiO_2-ZrO_2 Catalysts

Cu[a] wt %	crystallite size[b] (nm)	Cu metal area[b] (m^2/g_{Cu})	% dispersion[b]	% conversion	% selectivity of cyclohexanone	% selectivity of cyclohexene	TOF (s^{-1})
1.0	2.78	241	27	22	3	97	0.47
2.6	2.01	334	52	26	28	72	0.16
5.1	1.78	378	58	28	59	41	0.06
10.8	2.84	236	37	33	77	23	0.07
16.8	4.5	149	23	35	87	13	0.08
21.6	4.9	138	21	33	88	12	0.06

[a] Calculated from atomic absorption spectroscopy. [b] Calculated from N_2O decomposition.

TABLE 5: Dispersion, Copper Metal Area, BET Surface Area, TPD of NH_3, and Dehydrogenation Activity Results for Various Copper-Supported Catalysts

catalyst	BET surface area (m^2/g)	% dispersion[a]	Cu metal area[a] (m^2/g_{cu})	total NH_3 uptake[b] (μmol/g)	% conversion	% selectivity
10% Cu/ZrO_2	38	18.4	119	598	31	98
10% Cu/TiO_2	35	15.8	102	430	13	91
10.8% Cu/TiO_2-ZrO_2	128	37.0	236	717	33	77

[a] Calculated from N_2O decomposition. [b] Calculated from temperature programmed desorption of NH_3.

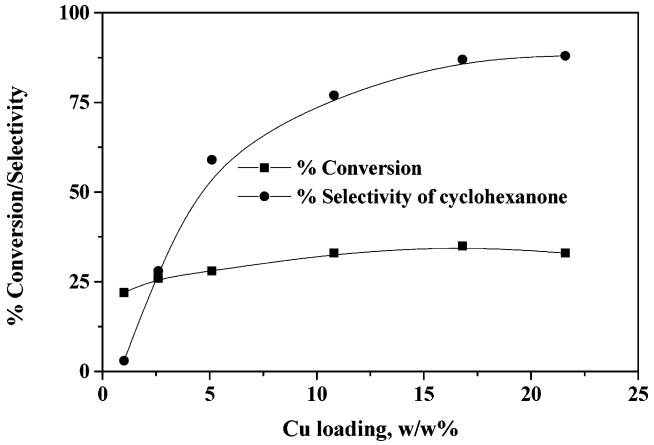

Figure 8. Dehydrogenation of cyclohexanol over various CuO/TiO_2-ZrO_2 catalysts (reaction temperature 523 K, gas hourly space velocity 6720 h^{-1}).

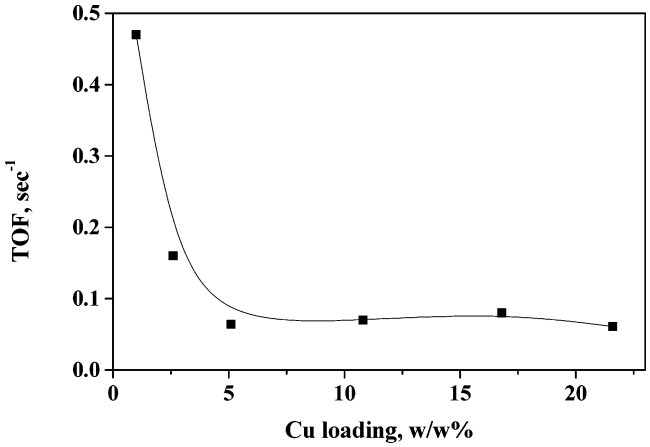

Figure 9. Relation between turn over frequency and copper loading.

dispersion and metal areas are decreased, and crystalline size is increased. This is also in good agreement with XRD and TPR.

The catalytic properties during the vapor-phase dehydrogenation of cyclohexanol exhibited by various CuO/TiO_2-ZrO_2 catalysts are shown in Figure 8. As can be seen from Figure 9, the cyclohexanol activity increases with increasing Cu loading up to 10.8 wt %. However, there is not much change in the activity observed with further increases in the Cu loading on TiO_2-ZrO_2. The conversion for 1 wt % Cu loading catalysts was 22% and increases to 33% as the copper loading increased to 10.8 wt %. The selectivity toward cyclohexanone was found to be very low for 1 wt % catalyst. However, further increases in copper loading on TiO_2-ZrO_2 increased the selectivity drastically toward 77% with 10.8 wt % loading. The selectivity was increased with further increases in the copper loading and increased only marginal at higher loadings. This may be due to increases in the crystallinity that makes more support surface available for dehydration activity at 523 K, which can be shown by XRD and ESR.

A comparison of the surface characterization and catalytic activity results of 10 wt % of Cu supported on titania, zirconia, and with the present Cu supported on titania−zirconia catalysts are reported in Table 5. The catalytic experiments were carried out under similar conditions employed for all the samples. The aim of this study is to see the effect of the support on the catalytic properties in relation to surface properties such as dispersion and metal area. The results of Table 5 clearly show that copper is well-dispersed on TiO_2-ZrO_2 support and also has a higher copper metal area. The conversion of cyclohexanol is also found to be higher in the case of the CuO/TiO_2-ZrO_2 catalyst compared to those of the CuO/TiO_2- and CuO/ZrO_2-supported catalysts. However, the selectivity during cyclohexanone formation is found to be less than the CuO/TiO_2 or CuO/ZrO_2 catalyst. This might be due to the higher acidity of

the TiO_2-ZrO_2 support as compared to pure ZrO_2 or TiO_2, leading to decreased dehydrogenation functionality during the vapor-phase dehydrogenation of cyclohexanol. The acidities of these three samples have been measured by the TPD of ammonia method and are reported in Table 5. Cyclohexene is the only byproduct formed during the vapor-phase dehydrogenation of cyclohexanol, and it is formed due to the acidic sites of supported Cu catalysts.

To find out the relation between the dehydrogenation of cyclohexanol and the copper loading, a plot of copper loading on TiO_2-ZrO_2 versus turnover frequency (TOF) is shown in Figure 9, where in the TOF is equal to the rate of cyclohexanol molecules converted per second per site of copper. TOF is constant for all the catalysts except for the 1 wt % of Cu catalyst. This may be due to the isolated copper ions present in the 1-wt % catalyst, which can be clearly shown from the UV-DRS results.

4. Conclusions

XRD results reveal the presence of crystalline CuO at high copper loadings (>10.8 wt %). N_2O decomposition is found to be a valuable method for measuring the dispersion of Cu on TiO_2-ZrO_2. Copper oxide disperses well on TiO_2-ZrO_2. The information obtained by UV-DRS, ESR, and TPR reveals the presence of two types of copper species on the TiO_2-ZrO_2 support. The dispersion of Cu determined by N_2O decomposition substantiates the findings of XPS and XRD. CuO supported on TiO_2-ZrO_2 is highly active for the vapor-phase dehydrogenation of cyclohexanol. The catalytic activity during the dehydrogenation of cyclohexanol is directly related to the dispersion of copper.

Acknowledgment. G.V.S. thanks the Council of Scientific and Industrial Research for a Senior Research Fellowship. D.N. thanks the Director, IICT, for the Junior Research Fellowship.

References and Notes

(1) Fabina, M. T.; Schmal, M. *Appl. Catal., A* **1997**, *163*, 153.
(2) Fridman, V. Z.; Davydov, A. A. *J. Catal.* **2000**, *195*, 20.
(3) Chang, H. F.; Slague, M. A. *J. Mol. Catal.* **1994**, *88*, 223.
(4) Kim, T. W.; Song, M. W.; Koh, H. L.; Kim, K. L. *Appl. Catal., A* **2002**, *210*, 35.
(5) Centi, G.; Perathoner, S. *Appl. Catal., A* **1995**, *132*, 179.
(6) Dandekar, A.; Vannice, M. A. *Appl. Catal., B* **1999**, *22*, 179.
(7) Matsuoka, M.; Ju, W.; Takahashi, K.; Yamashita, H.; Anpo, M. *J. Phys. Chem. B* **2000**, *104*, 4911.
(8) Praliaud, H.; Mikhailenko, S.; Chajar, Z.; Primet, M. *Appl. Catal., B* **1998**, *16*, 359.
(9) Radtke, F.; Koeppel, R. A.; Minardi, E. G.; Baiker, A. *J. Catal.* **1997**, *167*, 127.
(10) Martinez-Arias, A.; Fernandez-Garcia, M.; Galvez, O.; Coronado, J. M.; Anderson, J. A.; Conesa, J. C.; Soria, J.; Munuera, G. *J. Catal.* **2000**, *195*, 207.
(11) Brands, D. S.; Poels, E. K.; Bliek, A. *Appl. Catal., A* **1999**, *184*, 279.
(12) Chen, C.; Cheng, W.; Lin, S. *Catal. Lett.* **2000**, *68*, 207.
(13) Choi, K. J.; Vannice, M. A. *J. Catal.* **1991**, *131*, 22.
(14) Szanyi, J.; Goodman, D. W. *Catal. Lett.* **1993**, *21*, 165.
(15) Trimm, D. L.; Onsan, Z. I. *Catal. Rev.* **2001**, *43*, 31.
(16) Dandekar, A.; Vannice, M. A. *J. Catal.* **1998**, *178*, 621.
(17) Chen, W. S.; Lee, M. D.; Lee, J. F. *Appl. Catal.* **1992**, *83*, 201.
(18) Jeon, G.; Chaung, J. *Appl. Catal.* **1994**, *115*, 29.
(19) Gilson, C. A. U.S. Patent 3,998,884, 1976.
(20) Chen, W.; Lee, M.; Lee, J. *Appl. Catal.* **1992**, *83*, 201.
(21) Chan, H. F.; Saleque, M. *Appl. Catal.* **1993**, *103*, 233.
(22) Sivaraj, Ch.; Reddy, B. M.; Rao, P. K. *Appl. Catal.* **1988**, *45*, 111.
(23) Uemichi, Y.; Shouji, L.; Sugioka, M.; Kamazuka, T. *Bull. Chem. Soc. Jpn.* **1995**, *68*, 385.
(24) Murakami, Y.; Iwayama, K.; Uchida, H.; Hattori, T.; Tagawa, T. *J. Catal.* **1981**, *71*, 257.
(25) Vireland, G. E. *J. Catal.* **1988**, *111*, 1.
(26) Cadus, L. E.; Arrua, L. A.; Gorriz, G. F.; Riarola, J. B. *Ind. Eng. Chem. Res.* **1988**, *27*, 224.
(27) Matsuda, S.; Kato, A. *Appl. Catal.* **1983**, *8*, 149.
(28) Hattori, H.; Itoh, M.; Tanabe, K. *J. Catal.* **1976**, *41*, 46.
(29) Nakano, Y.; Hattori, H.; Tanabe, K. *J. Catal.* **1979**, *57*, 1.
(30) Wu, J. C.; Chung, C. S.; Ay, C. L.; Wang, I. *J. Catal.* **1984**, *87*, 98.
(31) Wang, I.; Wu, J. C.; Chung, C. S. *Appl. Catal.* **1985**, *16*, 89.
(32) Arata, K.; Akutagawa, S.; Tanabe, K. *Bull. Chem. Soc. Jpn.* **1976**, *49*, 390.
(33) Wang, I.; Chang, W. F.; Shiau, R. J.; Wu, J. C.; Chung, C. S. *J. Catal.* **1983**, *83*, 428.
(34) Hirashima, Y.; Nishiwaki, K.; Miyakoshi, A.; Tsuiki, H.; Ueno, A.; Nakabayashi, H. *Bull. Chem. Soc. Jpn.* **1988**, *61*, 1945.
(35) Fung, J.; Wang, I. *J. Catal.* **1991**, *130*, 577.
(36) Hashimoto, K.; Masuda, T.; Kashihara, H. *Appl. Catal., A.* **1991**, *75*, 331.
(37) Mariscal, R.; Rojas, S.; Gomez-Cortes, A.; Diaz, G.; Perez, R.; Fierro, J. L. G. *Catal. Today* **2002**, *75*, 385
(38) Bond, G. C.; Namijo, S. N. *J. Catal.* **1989**, *118*, 507.
(39) Chen, L.; Horiuchi, T.; Osaki, T.; Mori, T. *Appl. Catal., B* **1999**, *23*, 259.
(40) Velu, S.; Suzuki, K.; Okazaki, M.; Kapoor, M. P.; Osaki, T.; Ohashi, F. *J. Catal.* **2000**, *194*, 373.
(41) Mendes, F. M.T.; Schmal, M. *Appl. Catal., A* **1997**, *151*, 393.
(42) Little, L. H. *Adsorption and Infrared Spectroscopy*.
(43) Marion, M. C.; Garbowskim, E.; Primet, M. *J. Chem. Soc., Faraday Trans.* **1990**, *86*, 3027.
(44) Iwamoto, M.; Yahiro, H.; Tanda, K.; Mizuno, Y.; Mine, Y.; Kagawa, S. *J. Phys. Chem.* **1991**, *95*, 3727.
(45) Centi, G.; Perathoner, S.; Billing, D.; Giamello, E. *J. Catal.* **1995**, *151*, 75.
(46) Dow, W.; Wang, Y.; Huang, T. J. *J. Catal.* **1996**, *160*, 155.
(47) Indovina, V.; Occhiuzzi, M.; Pietrogiacomi, D.; Tuti, S. *J. Phys. Chem. B.* **1999**, *103*, 9967.
(48) Ratnasamy, P.; Srinivas, D.; Satyanaryana, C. V. V.; Manikandan, P.; Senthil Kumaran, R. S.; Sachin, M.; Shetti, V. N. *J. Catal.* **2004**, *221*, 455.
(49) Chary, K. V. R.; Seela, K. K.; Sagar, G. V.; Sreedhar, B. *J. Phys. Chem. B* **2004**, *108*, 658.
(50) Tseng, I.-H.; Chang, W.-C.; Wu, Jeffrey C. S. *Appl. Catal., B* **2002**, *37*, 37.
(51) Bechara, R.; Aboukais, A.; Bonnelle, J.-P. *J. Chem. Soc., Faraday Trans.* **1993**, *89*, 1257.
(52) *Practical Surface Analysis by Auger and X-ray Photoelectron Spectroscopy*; Brigs, D., Seah, M. P., Eds.; Wiley: New York, **1983**.
(53) Yan, J. Y.; Lee, G. D.; Sachtler, W. M. H.; Kung, H. *J. Catal.* **1996**, *161*, 43.
(54) Fierro, G.; Lo Jacono, M.; Inversi, M.; Porta, P.; Lavecchia, R.; Cioci, F. *J. Catal.* **1994**, *148*, 709.
(55) Zhou, R.; Yu, T.; Jiang, X.; Chen, F.; Zheng, X. *Appl. Surf. Sci.* **1999**, *148*, 263.
(56) Delk, F. S.; Vavere, A. *J. Catal.* **1994**, *147*, 322.
(57) Kundakovic, L. J.; Flytzani-Stephanopoulos, M. *Appl. Catal., A* **1998**, *171*, 13.
(58) Bantley, J.; Burch, R.; Chappel, R. J. *Appl. Catal.* **1988**, *43*, 99.
(59) Evans, J. W.; Wainwright, M. S.; Bridgewadr, A. J.; Yang, N. *Appl. Catal.* **1983**, *7*, 75.